Future Sustainability
Open Access Journal
ISSN 2995-0473

February 2025| Volume 03 | Issue 01 | Pages 36-48

Journal homepage: https://fupubco.com/fusus

https://doi.org/10.55670/fpll.fusus.3.1.4

Future Publishing LLC

Article

Integration of a biomass-fired thermal plant with solar-turbine and solar-assisted dryer for multi-energy generation

John Isaac[1]*, Fidelis Abam[2], Bassey Okon[3], Patrick Adah[2], Uduma Okoro[4], Cyprian Igube[5], Nnaemeka S. Obuka[6], Archibong Archibong-Eso[7]

[1]Department of Mechanical Engineering, University of Cross River State, Calabar, Nigeria
[2]Department of Mechanical Engineering, University of Calabar, Calabar, Nigeria
[3]Department of Mechanical Engineering, Federal University of Technology, Ikot Abasi, Ikot Abasi, Nigeria
[4]Department of Mechanical Engineering, Michael Okpara University of Agriculture Umudike, Umuhia, Nigeria
[5]Department of Mechanical Engineering, Covenant University Ota, Ota, Nigeria
[6]Department of Mechanical Engineering, Enugu State University of Science and Technology Enugu, Enugu, Nigeria
[7]Department of Mechanical Engineering, Bermingham University Dubai Campus, Dubai, United Arab Emirates

ARTICLE INFO

Article history:
Received 12 December 2024
Received in revised form
15 January 2025
Accepted 29 January 2025

Keywords:
Biomass, Environmental, Sustainability, Turbine, Organic Rankine Cycle (ORC)

*Corresponding author
Email address:
newton4y@yahoo.com

DOI: 10.55670/fpll.fusus.3.1.4

ABSTRACT

The study analyzed the thermodynamics and environmental performance of a biomass-based solar-assisted trigeneration system for power, cooling, and hot water production. The system uses municipal waste in an incinerator and a solar tower with a gas turbine supplemented by natural gas. It includes an Organic Rankine Cycle (ORC) for power, a vapor absorption system (VAS) for refrigeration, and a gas turbine. The analysis focused on thermodynamic, exergoeconomic, and thermo-environmental perspectives, considering indicators like the exergetic utility index (EUI), exergo thermal index (ETI), waste exergy ratio (WER), and sustainability index (SI). Simulation results show a net output of 6.128 MW, a cooling capacity of 131.1 kW, and a cooling water flow of 65.14 kg/s. The energy and exergy efficiencies are 66.68% and 53%, respectively. The solar tower helps reduce natural gas use by 633.6 kg/h, lowering carbon emissions. Exergy destruction is highest in the incinerator and combustion chamber. The exergoeconomic analysis shows minimal cost reduction in the gas turbine air compressor and incinerator. Thermo-environmental indicators were recorded as EUI 0.6992, ETI 0.9161, WER 1.092, and SI 0.6109, reflecting the system's environmental friendliness due to efficient energy use and low discharge temperatures.

1. Introduction

Energy availability and sustainability are critical indicators of societal well-being, directly impacting the economic growth and development of both developed and developing nations [1]. As energy sustainability depends on population size, its availability must be continually enhanced to meet the needs of society while fostering industrialization. However, many energy resources are finite, and the reliance on fossil fuels for energy conversion leads to environmental pollution [2-4]. To meet increasing energy demands while ensuring environmental sustainability, exploring renewable energy sources beyond conventional non-renewables, which account for about 65% of global power generation [5]. Additionally, improving the efficiency of existing non-renewable-based energy systems, which dominate global power production, is crucial. In this context, tri- and multigeneration energy systems have been proposed to generate multiple products from a single energy source with significantly higher efficiencies. Various configurations of these advanced systems have been extensively studied regarding thermodynamic performance and economic implications, including thermoeconomic, optimization, and environmental impact assessment. While some robust multigeneration systems are based on non-renewable energy

sources [6], most rely on solar energy, which is inherently [7-9]. Owing to the unpredictability of solar radiation and wind velocity, multigeneration systems dependent on renewable energy often exhibit lower efficiency and are unavailable during periods of low solar radiation. However, advanced solar-powered renewable energy systems have demonstrated relatively high energy and exergy efficiencies, significantly increasing overall output [10, 11]. Similarly, Ref [12] presented a solar-powered system for power generation, hydrogen production, cooling, and drying, improving energy and exergy efficiencies. In another study, nanofluids were utilized to enhance the performance of a solar-powered system that produced only electricity and cooling [13]. Past studies on solar-powered trigeneration and multigeneration energy systems have demonstrated slight improvements in energy efficiency and product output [14,15]. Other studies that involved hybrid energy systems, including solar-biomass and biomass-Kalina systems and combination with fuel oxide cells, are studied by [16-19]. Despite the successes achieved in previous studies, the efficiencies of combined systems may not show significant improvements in many cases. One potential issue with biomass-based systems is that, during the initial stages of biomass combustion in the incinerator, the required temperature may not be immediately reached, which can hinder adequate combustion. This delay in achieving the necessary temperature can lead to low overall efficiency, particularly when high-temperature working fluids are involved, resulting in a lower source heat exit temperature. A biomass/solar multigeneration system for power, cooling, and heating has been developed to address this limitation. This system incorporates a solar-assisted biomass preheating unit and a solar turbine in the topping cycle. The solar biomass preheating system completely dries the biomass before it enters the incinerator and provides additional heat, enhancing the combustion process. Consequently, this study proposes a novel energy configuration that combines municipal waste and solar power to generate sustainable power, cooling, and heating. The system utilizes solar energy as a backup for a gas turbine, reducing natural gas consumption. At the same time, municipal waste is dried to fuel both an Organic Rankine Cycle (ORC) for power generation and a vapor absorption chiller for cooling.

2. System description

The proposed energy generation system driven by municipal waste and solar irradiance is shown in Figure 1 (Appendix). The system comprises four subsystems, including an organic Rankine cycle (ORC), a single effect vapor absorption chiller (VAC), a solar-assisted gas turbine (SGT), a water heater, and a solar dryer drying the municipal waste before the commencement of the cycle and also for supplying additional heat to the incinerator. In its operation, municipal waste is dried and fed into an incinerator (points 1 and 2) in the presence of limited air. In this arrangement, syngas at a temperature T_3 and pressure P_3 is generated to drive the ORC for power generation. The exhausted syngas from the ORC vapor generator are further passed through a desorber (points 6 and 11) to power the VAC system for cooling. Furthermore, the exhausted syngas from the desorber is partly used (in addition to a solar collector) to dry the municipal waste before it enters the incinerator. The cooling water from refrigeration produced at the VAC acts as a cooling medium to reduce the ambient temperature of the air entering the air compressor to nearly ISO condition. In this arrangement, the air compressor work requirement is significantly reduced. The compressed air is heated by a solar collector (points 28 and 29), and the heat content is further enhanced with a heat exchanger, which collects heat from the expanding turbine. The heated air expands in a turbine, producing electrical energy, while the solar tower further heats the exhaust from the turbine for domestic water heating.

3. Methodology

3.1 Energy and exergy system modelling

The energy flow balance for the components in the steady state flow for the kth component are expressed in Eq. (1) [2, 17].

$$\sum \dot{Q}_k + \sum \dot{m}_i \left(h_1 + \frac{C_i^2}{2} + gz_1\right) = \sum \dot{m}_e \left(h_0 + \frac{C_0^2}{2} + gz_0\right) + \sum W \quad (1)$$

Where the rate of heat input to the system and the mass influx are denoted as $\dot{Q}_k$ and $\dot{m}_i$, respectively. Further, the enthalpy, kinetic energy, and potential energy of the stream is denoted as h_1, $\frac{C_i^2}{2}$, and gz_1, in that order. In the absence of any material loss to the environment, the steady state mass flow balance can also be written:

$$\sum \dot{m}_i = \sum \dot{m}_0 \quad (2)$$

Furthermore, using the second law of thermodynamics, the overall exergy system balance for a control system in a steady state, neglecting potential, kinetic, and electrical energy, is defined as:

$$\dot{E}_{xd} = \sum_k \left(1 - \frac{T_0}{T_k}\right) \dot{Q}_k - \dot{W}_{cv} + \sum_i \left(n_i \dot{E}x_i\right) - \sum_e \left(n_e \dot{E}x_e\right) \quad (3)$$

Where $\dot{E}_{xd}$ is the exergy destruction rate, $\left(1 - \frac{T_0}{T_k}\right) \dot{Q}_k$ represent the rate of exergy flow accompanied by the heat transfer, $\dot{W}_{cv}$ is the rate of work done within the control volume, $n_i \dot{E}x_i$ and $n_e \dot{E}x_e$ is the exergy flow rate in and out of the control volume [17]. The energy and exergy balances of the system are shown in Table 1 (Appendix) for energy and Table 2 (Appendix) for exergy.

3.2 Exergo-economic modelling of the system

Exergoeconomic analysis is employed in this research to evaluate the system's cost-effectiveness in terms of its operating cost and the price associated with the generated energy. The general cost balance for a control volume for $\boldsymbol{k^{th}}$ component is obtained as [17, 20]:

$$\dot{C}_{q,k} + \sum_i \dot{C}_{i,k} + \dot{Z}_k = \sum_e \dot{C}_{e,k} + \dot{C}_{w,k} \quad (4)$$

Where $\dot{C}_{q,k}$, is the cost associated with the j^{th} the sum of exergy streams to the system20's k^{th} component $\sum_i \dot{C}_{i,k}$, and the levelized cost rate for the k^{th} component, $\dot{Z}_k$. The other terms are the cost associated with the j^{th} the sum of exergy streams from the system's k^{th} component $\sum_e \dot{C}_{e,k}$, while the work associated with the k^{th} component is $\dot{C}_{w,k}$. The purchase equipment cost (PEC) and other cost functions are presented in Table 3 (Appendix) [17, 21, 22]. The cost rate $\dot{Z}_k$ for the components are related as:

$$\dot{Z}_k = \frac{PECF \times CRF \times \phi}{N \times 3600} \quad (5)$$

$$CRF = \frac{i|1+i|^n}{|1+i|^n-1} \quad (6)$$

PECF, CRF, and ϕ represent the purchase of equipment cost function, capital recovery factor, and maintenance factor, respectively. The system's annual operational hours are denoted with N, while n (years) is the expected life of the plant. The general relationship for evaluating the specific cost of the product for the k[th] component $c_{P,k}$ ($\$/kJ$), and that of fuel $c_{F,k}$ ($\$/kJ$), as well as the exergoeconomic factor, f is presented in Eqs (7) to (9), respectively [22].

$$c_{P,k}\ (\$/kJ) = \frac{\dot{C}_{P,k}}{\dot{E}_{P,k}} \quad (7)$$

$$c_{F,k}\ (\$/kJ) = \frac{\dot{C}_{F,k}}{\dot{E}_{F,k}} \quad (8)$$

$$f = \frac{\dot{Z}_k}{\dot{Z}_k + \dot{C}_{D,k}} \quad (9)$$

The cost of exergy destruction is expressed with the relationship:

$$\dot{C}_{D,k} = c_{P,k}E_{D,k} \quad (10)$$

3.3 Environmental and sustainability analysis

An environmental assessment is conducted for the system using established exergoenvironmental indicators. In this study, additional exergy and thermal-based environmental indicators are utilized to quantify the environmental sustainability of the proposed system. The assessment considers the emissions of CO, NO_x, and CO_2, along with several other indices. These include the fuel effect factor. F_{ef}, the exergetic sustainability index ESI, and specific emissions from carbon dioxide $Co_{2(s)e}$. Others are the exergetic utility index, EUI, and the exergo-thermal index ETI [2].

4. Results and discussion

The thermodynamic analysis results of the system using n-octane are presented for state points, components, and the overall system based on the design conditions in Table 4. Simulated conditions were used to derive performance indices, with the following simplifying assumptions. Ambient air temperature and pressure were 27°C and 1.013 bar, respectively; the Condenser water inlet temperature was 20°C, based on local weather conditions; system boundaries assumed adiabatic, neglecting heat losses, all computations assumed steady-state conditions; pressure drops in components were neglected, combusted gases treated as ideal gases, and turbine and pump isentropic efficiencies set to 80% [6, 19].

The temperature of the compressed combustion products entering the gas turbine was designed at 930°C, significantly enhanced by solar heat. For preliminary simulation, solar energy was 7542 kW, based on an energy balance between the combustion unit and solar tower, adjusted for changing weather. In this setup, the natural gas input to the combustion chamber is influenced by solar irradiance. The natural gas flow rate for the preliminary design was 0.61 kg/s. The results of the thermodynamic state point characteristics based on the operating input data in Table 4 are presented in Table 5.

Table 4. Design conditions for the plant [2, 6, 17]

Property	Value	Unit
Gasification temperature	450	°C
ORC turbine inlet temperature	200	°C
ORC turbine inlet pressure	10.0	bar
ORC turbine expansion ratio	5.0	Dim.
VAS upper operating pressure	0.074	bar
VAS desorber temperature	85	°C
VAS lower operating pressure	0.0068	bar
VAS evaporator temperature	3.0	°C
Gas turbine pressure ratio	5.0	Dim.
Gas turbine inlet temperature	930	°C
Solar heat	7542	kW

The system performance under various operating conditions is summarized in Table 6. The results show that the overall turbine network output is 6128 kW, with individual outputs for the ORC turbine and the gas turbine calculated at 16516 kW and 10388 kW, respectively. In terms of system efficiencies, the thermal efficiency is 66.68%, and the exergy efficiency is 53.21%. The average temperature of the hot water generated was 75°C, and the refrigerating capacity achieved did not exceed 131.1 kW. These values for hot water temperature and refrigerating capacity were sufficient to maintain human comfort and provide the necessary energy to support the local economy. The effect of the expansion ratio on turbine back pressure and condenser cooling water flow rate is shown in Figure 2. Higher expansion ratios reduce turbine back pressures and cooling water flow. The relationship between the expansion ratio and turbine back pressure is linear, with a gradient proportional to the square of the back pressure relative to the turbine inlet pressure. Although higher back pressures reduce heat transfer demands, the relationship between cooling water flow and expansion ratio is nearly parabolic.

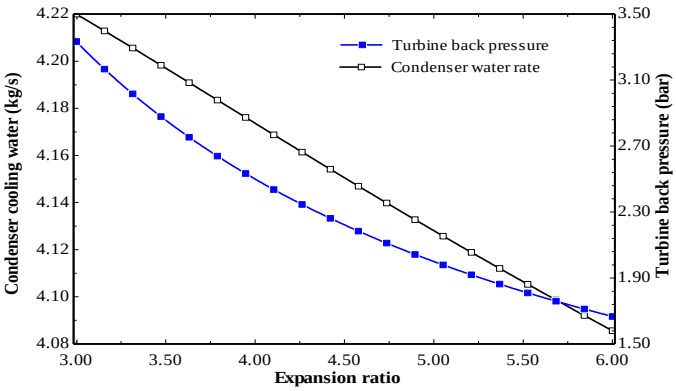

Figure 2. Effect of expansion ratio on turbine back pressure and condenser cooling water flow rate

Table 5. Thermodynamic state point characteristic of the integrated biomass solar-assisted system

S/No	Ex (kW)	h (kJ/kg)	m (kg/s)	P (bar)	s (kJ/kg.K)	T (°C)
1	0.0000	298.4	4.433	1.013	5.695	25.00
2	16273	-8442	0.750	1.013	1.362	25.00
3	11.4400	336.6	5.183	1.013	5.816	63.00
4	-	-	-	-	-	-
5	871.50	738.4	5.183	1.013	6.607	450.00
6	439.60	584.1	5.183	1.013	6.369	304.90
7	327.50	454.7	3.200	10.00	1.183	200.00
8	299.60	446	3.200	2.000	1.183	152.00
9	80.49	203.2	3.200	2.000	0.598	110.00
10	84.84	204.9	3.200	10.00	0.598	110.40
11	5.996	325.9	5.183	1.013	5.783	52.40
12	7.197	2658	0.056	0.074	8.506	85.00
13	0.0922	171.1	0.056	0.074	0.584	40.30
14	0.5504	171.1	0.056	0.0068	0.623	1.70
15	-11.71	2503	0.056	0.0068	9.114	1.70
16	0.113	92	0.418	0.0068	0.199	34.60
17	0.115	92.01	0.418	0.0742	0.199	34.60
18	2.199	156.3	0.418	0.0742	0.398	67.00
19	2.048	238.5	0.362	0.0742	0.443	85.00
20	-0.72	169.3	0.362	0.0742	0.236	45.00
21	5.149	169.3	0.362	0.0068	0.182	35.00
22	0.237	83.3	1.337	1.0130	0.294	20.00
23	3.593	187.9	1.337	1.0130	0.637	35.00
24	0.000	298.4	5.933	1.0130	5.695	25.00
25	5.090	276.3	5.933	1.0130	5.618	3.00
26	0.000	298.4	41.56	1.0130	5.695	25.00
27	0.608	295.7	47.49	1.0130	5.686	22.20
28	9069	514.4	47.49	5.0650	5.779	237.70
29	12719	671.5	47.49	5.0650	6.048	387.70
30	14305	730.5	47.49	5.0650	6.134	442.70
31	30276	43852	0.62	5.0650	-	25.00
32	32613	1281	48.11	5.0650	6.719	930.00
33	14169	938.2	48.11	1.0130	6.853	631.40
34	12319	880	48.11	1.0130	6.787	579.30
35	7709	724.8	48.11	1.0130	6.588	437.50
36	578.5	391.6	48.11	1.0130	5.967	117.50
37	10.46	83.3	58.93	1.0130	0.294	20.00
38	1316	355.3	58.93	1.0130	1.132	85.00
39	42.58	271.5	4.13	1.0130	0.892	65.00
40	0.7325	83.3	4.13	1.0130	0.294	20.00
41	1.6250	55.42	-	1.0130	-	34.00
42	4.2020	187.9	1.56	1.0130	0.637	45.00
43	-	-	-	-	-	-
44	-	-	-	-	-	-
45	27.65	358.8	5.18	1.0130	5.880	85.00
46	1.101	83.3	6.20	1.0130	0.294	20.00
47	63.99	271.5	6.20	1.0130	0.892	65.00
48	0.277	83.3	1.56	1.0130	0.294	20.00

The pinch point temperature at the lower side of the vapor generator (VG) affects the quantity of heated water for domestic use. An energy balance around the water heater, with constant exit temperature and fixed temperature along the VAS desorber, shows that the pinch point temperature influences hot water production, as seen in Figure 3. The hot water flow increased slightly from 5.4 to 6.6 kg/s with a 35°C rise in pinch point temperature. Additionally, the VG stack temperature rose linearly with the pinch point temperature, with each 10°C increase in pinch point temperature resulting in a 10°C rise in VG stack temperature. The circulation ratio of ammonium water solution around the generator, heat exchanger, and absorber in the vapor absorption system is investigated on the cooling rate of the evaporator and shown in Figure 4. Between circulation ratios of 0.62 and 0.68, the cooling rate was constant at 131.16 kJ/s.

The constant rate of evaporator cooling at varying circulation rates results from the constant mass flow rate of the refrigerant water. Therefore, any variation of the circulation ratio of rich ammonia around the generator and absorber only increases the quantity of heat to be dissipated by the absorber.

The effect of solar irradiance on natural gas consumption in the combustion chamber for achieving the required turbine power is shown in Figure 5. The solar tower reduces natural gas usage due to the balance between solar energy and compressed air from the compressor. Without solar-assisted heat addition, the system requires 0.856 kg/s of natural gas. Solar assistance reduces the natural gas necessary by 0.176 kg/s, reaching 0.680 kg/s under design conditions.

Table 6. Summary of performance indices of the plant

Performance index	Value	Unit
ORC turbine output	27.85	kW
ORC condenser heat rate	777	kW
ORC vapour generator heat input	799.5	kW
ORC turbine expansion ratio	33	dim.
VAS generator heat input	170.4	kW
VAS refrigeration rate	131.1	kW
Gas turbine compressor work	10388	kW
Gas turbine output	16516	kW
Total quantity of domestic hot water	65.14	kg/s
Average temperature of domestic hot water	75	°C
System total thermal efficiency	66.68	%
System total exergy efficiency	53.21	%
Overall turbine network output	6128	kW

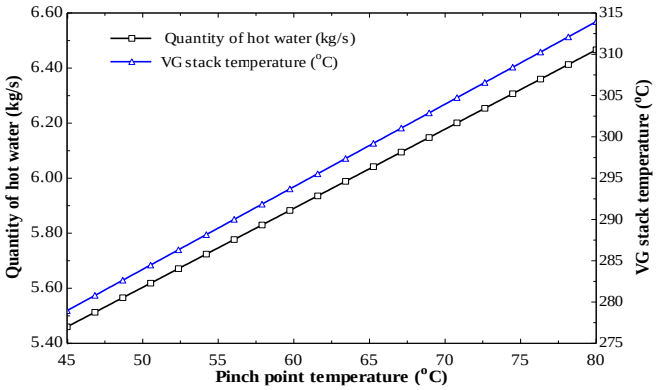

Figure 3. Effect of pinch point temperature on quantity of hot water and VG stack temperature

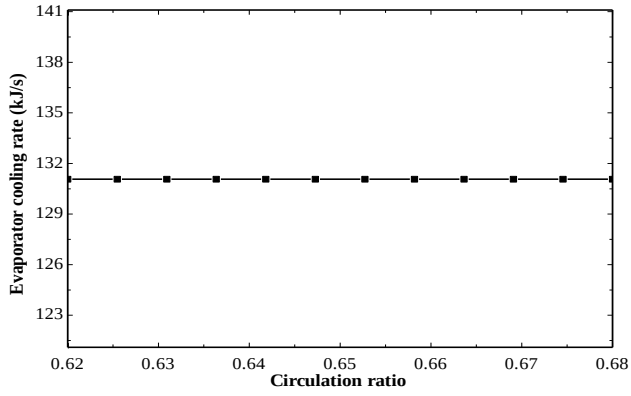

Figure 4. Circulation ratio effect on cooling rate in the VAS

Table 7 presents the initial investment, monetary flow rate, and levelized capital cost for all the components. Equipment costs align with operating parameters from published literature. The results show that component costs depend on power output, input, and heat transfer between components and surroundings, particularly for condensers, heat exchangers, and water heaters. The PEC for the topping cycle components, including the solar-powered turbine, ranges up to 10^5 dollars. Table 8 presents the exergoeconomic parameters of the system, helping us to understand cost formation, exergy destruction, and performance factors like the exergoeconomic factor. It shows fuel and product costs, exergy destruction and related costs, component-level cost rates, and exergoeconomic factors. Exergy destruction in the incinerator and gas turbine combustion chamber is significant due to temperature fluctuations, suggesting a need for incinerator design improvement. The exergoeconomic factor relates exergy destruction cost to component cost rates. A low factor indicates potential cost savings through improved efficiency. High factors suggest reduced investment costs at the expense of efficiency.

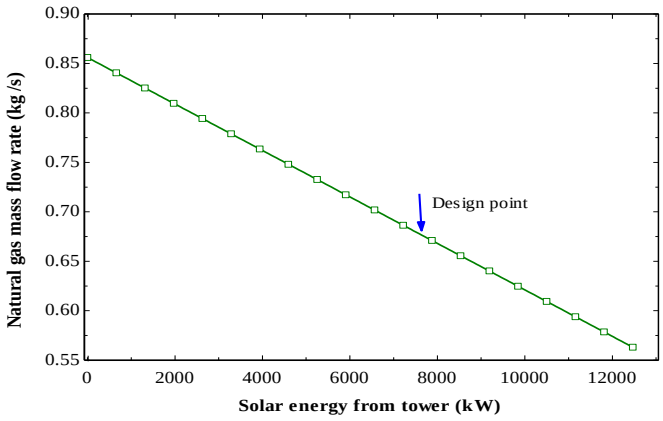

Figure 5. Relationship between solar energy from the tower and mass flow rate of fuel

The environmental analysis quantifies emissions from the gas turbine section due to fossil fuel combustion supporting solar radiation. CO and NO_x emissions are analyzed with respect to the adiabatic flame temperature of the combustion chamber. Emission quantities at varying combustion temperatures are shown in Figure 6. The primary zone temperature affects emissions, especially at temperatures between 1200 K and 2300 K, where CO emissions are low but NO_x emissions are high. For this temperature range, 3.4 grams/year CO and 718,005,617 grams/year NO_x were recorded at lower temperatures, 108.69 grams/year CO, and 23,281,266,383 grams/year NO_x at higher temperatures. For primary zone temperatures above 2300 K, NO_x emissions increase by 18,875.7 tons/yr for every 50°C rise in combustion chamber temperature at a compression ratio of 5 (Figure 7). These emissions are high due to the elevated temperatures and compressor work.

From [2, 23], it is crucial to maintain moderate turbine inlet temperatures while increasing the air compression ratio to achieve high turbine output with reduced NO_x emissions. Similar studies have shown that reducing NO_x emissions is possible at higher compression pressure ratios. As noted from the study, high compression pressure ratios before combustion significantly reduce NO_x emissions in gas turbine systems, as shown in Figure 8. The pressure values at the combustion chamber inlet, related to ambient pressure and compression ratio, were considered. For this system, emissions decreased by 3.943% for every 2-unit increase in compression ratio.

Table 7. Initial investment, monetary flow rate, and levelized capital cost rate

Plant component	PEC [USD]	Levelized cost per year [USD/yr.]	Levelized cost per hour [USD/hr.]
Cooler	8910	1583	0.20980
GT ACP	150989	26829	3.55500
G TCC	49923	8871	1.17500
GT HEX	5380	956	0.12670
GT SOLAR TWR	15014	2668	0.35350
GT TURB	309339	54967	7.28300
INCINERATOR	5812000	1032000	136.80000
ORC CND	7964	1415	0.18750
ORC PUMP	412	73	0.00970
ORC TURB	57593	10234	1.35600
ORC VG	10208	1814	0.24030
VAS ABS	5758	1023	0.13560
VAS CND	3955	703	0.09312
VAS DEBS	7556	1343	0.17790
VAS EVP	6853	1218	0.16130
VAS HEX	5380	956	0.12670
VAS PUMP	132	23	0.00311
VAS VLV1314	188	33	0.00442
VAS VLV2021	188	33	0.00442
WASTE DRYER	5380	956	0.12670
WATER HEATER 1	5758	1023	0.13560
WATER HEATER 2	5380	956	0.12670

Table 8. Summary of exergoeconomic parameters of the plant

Plant component	$\dot{C}_F$ ($/GJ)	$\dot{C}_P$ ($/GJ)	$\dot{E}_D$ (MW)	$\dot{C}_D$ ($/hr.)	Z ($/hr.)	$Z+\dot{C}_D$ ($/hr.)	f (%)
COOLER	0	95.6314	0.004487	0.0000000	0.2098	0.2098	100.000
GT ACP	0.141549	0.270985	1.320000	0.6726422	3.555	4.2276	84.089
G TCC	0.063458	0.096743	11.970000	2.7345517	1.175	3.9096	30.055
GT HEX	0.096697	0.134426	0.263200	0.0916221	0.1267	0.2183	58.034
GT S. TWR	0.09681	0.026941	0.960600	0.3347830	0.3535	0.6883	51.360
GT TURB	0.096719	0.141537	1.928000	0.6713040	7.283	7.9543	91.560
Incinerator	0.017927	43.96825	15.413000	0.9947229	136.8	137.7947	99.278
ORC CND	76.79142	403.2922	0.177300	49.0144272	0.1875	49.2019	0.381
ORC PUMP	75.9491	92.61388	0.000926	0.2530472	0.0097	0.2627	3.692
ORC TURB	76.80032	75.93258	0.000000	0.0000077	1.356	1.3560	99.999
ORC VG	42.85328	76.50911	0.189200	29.1882288	0.2403	29.4285	0.817
VAS ABS	66.3388	286.356	0.012820	3.0616684	0.1356	3.1973	4.241
VAS CND	2365.055	14857.2	0.005978	50.8978718	0.09312	50.9910	0.183
VAS DESB	49.12219	132.1435	0.014610	2.5836309	0.1779	2.7615	6.442
VAS EVP	0	8.775946	0.006061	0.0000000	0.1613	0.1613	100.000
VAS HEX	63.72904	101.3809	0.000678	0.1556416	0.1267	0.2823	44.875
VAS PUMP	75.92484	569.8841	0.000000	0.0000000	0.00311	0.0031	100.000
VAS VLV1314	11697.13	1776.99	0.000634	26.6975335	0.00442	26.7020	0.017
VAS VLV2021	18.34768	133.838	0.005864	0.3873269	0.00442	0.3917	1.128
WASTE DRYER	16.94903	25.51962	0.003714	0.2266153	0.1267	0.3533	35.860
WH 1	45.07944	281.0904	0.349100	56.6540397	0.1356	56.7896	0.239
WH 2	0.096776	0.555343	5.825000	2.0293970	0.1267	2.1561	5.876

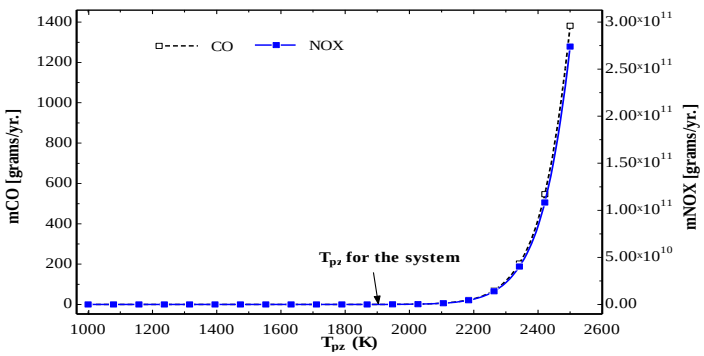

Figure 6. Effect of primary zone temperature on emissions

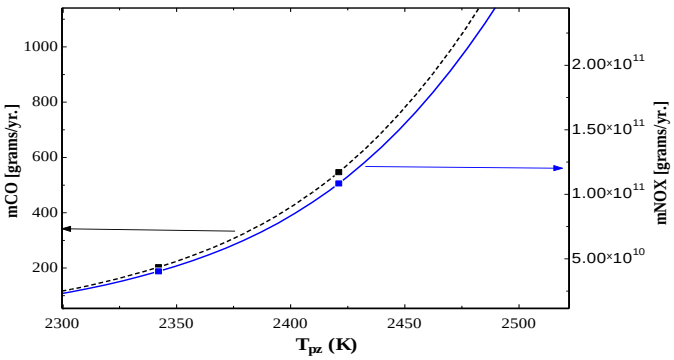

Figure 7. Effect of critically high primary zone temperature on emissions

Figure 9 shows similar results, aligning with the impact of primary zone temperature on NO_x emissions. Increasing turbine inlet temperatures (TITs) raise emissions, as TIT is directly linked to primary zone temperature. The system's exergy-based sustainability results are presented in Figure 10 and calculated based on total exergy destruction, system product, and plant exergy efficiency [24]. Environmental indices such as the exergetic utility index (EUI), exergo thermal index (ETI), waste exergy ratio (WER), and sustainability index (SI) were measured. At the design condition in Table 4, the EUI, ETI, WER, and SI were calculated at 0.6992, 0.9161, 1.092, and 0.6109, respectively.

The SI remains strong even with high exergy destruction from the incinerator and combustion chamber. Neglecting significant incinerator exergy destruction results in an SI value of 1.02. The EUI, measuring exergy resource utilization, was estimated at 0.6992, indicating good exergy efficiency. A 2% improvement in EUI was observed by adding a water heater in the system, reducing flue gas temperature by 110°C. The ETI of 0.9161 highlights the system's thermal impact; reducing the flue gas temperature to 50°C could enhance the ETI by 14.66%.

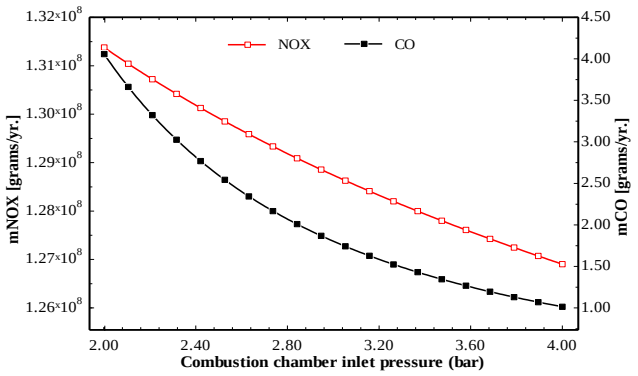

Figure 8. Effect of combustion chamber inlet pressure on emissions

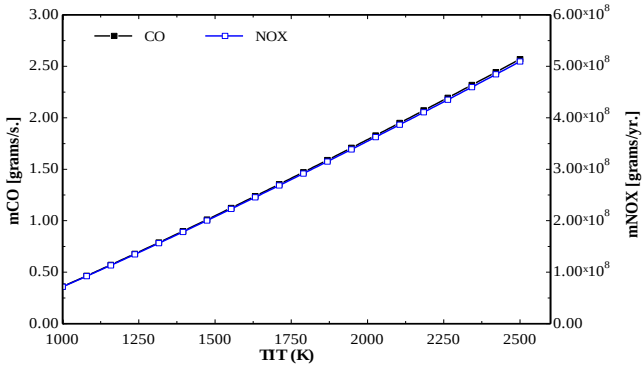

Figure 9. Effect of turbine inlet temperature (TIT) on emissions

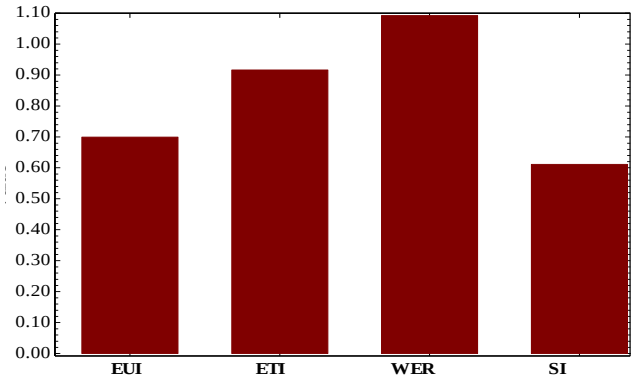

Figure 10. Exergetic sustainability indicators of the system

5. Conclusions

The study analyzed the thermodynamic, exergoeconomic, and thermo-environmental performance of a solar/biomass-based trigeneration energy system for heating, cooling, and power generation. The system's net output, cooling capacity, and cooling water flow rate were 6.128 MW, 131.1 kW, and 65.14 kg/s (at 75°C), respectively, with energy and exergy efficiencies of 66.68% and 44%. High ORC turbine expansion ratios reduced turbine back pressures and condenser cooling water. The cooling water quantity followed a parabolic relationship with the turbine expansion ratio. The stack temperature after the ORC vapor generator was linearly related to hot water from the domestic heater. The evaporator cooling rate remained constant across different ammonium water solution circulation ratios. However, reducing the VAS evaporator temperature by 13°C decreased compressor work requirements by 2000 kW. The solar tower reduced natural gas consumption by 633.6 kg/h, lowering carbon emissions. The incinerator and combustion chamber contributed significantly to exergy destruction. High exergoeconomic factors for some components indicated a need to reduce investment costs, particularly for the spray cooler, gas turbine air compressor, and incinerator. The system's environmental indices, EUI, ETI, WER, and SI, were estimated at 0.6992, 0.9161, 1.092, and 0.6109, respectively. The study concluded that the proposed energy system is highly sustainable and effectively reduces environmental impacts to a significant extent.

Ethical issue

The authors are aware of and comply with best practices in publication ethics, specifically with regard to authorship (avoidance of guest authorship), dual submission, manipulation of figures, competing interests, and compliance with policies on research ethics. The authors adhere to publication requirements that the submitted work is original and has not been published elsewhere.

Data availability statement

The manuscript contains all the data. However, more data will be available upon request from the authors.

Conflict of interest

The authors declare no potential conflict of interest.

References

[1] C. Chen, M. Pinar, T. Stengos. (2020). Renewable energy consumption and economic growth nexus: Evidence from a threshold model. Energy Policy, 139(2020) 111295.doi: 10.1016/j.enpol.2020.111295.

[2] F. I. Abam, O. E. Diemuodeke, E. B. Ekwe, M. Alghassab, O. D. Samuel, Khan, Z. A., et al. Exergoeconomic and environmental modeling of integrated Polygeneration power plant with biomass-based syngas supplemental firing. Energies 13(2020)6018-6027. doi:10.3390/en13226018.

[3] F. Johnsson, J. Kjärstad, J. Rootzén, J. The threat to climate change mitigation posed by the abundance of fossil fuels. Climate Policy, (2018)1-17. doi:10.1080/14693062.2018.1483885.

[4] J. G. J Olivier, J. A. H. W., Peters, K. M. Schure, K. M. Trends in global emissions of CO2 and other greenhouse gases: 2017 Report (PBL report no. 2674). PBL Netherlands Environmental Assessment Agency, Bilthoven, the Netherlands.

[5] D. Nikhil, A. Rajesh. Performance analysis of combined cycle power plant, Frontiers in Energy DOI 10.1007/s11708-015-0371-9.

[6] C. C Oko, H. I. Njoku. Performance analysis of an integrated gas-, steam- and organic fluid-cycle thermal power plant. Energy, 122(2017)431-443.

[7] Manente, G. (2016). High performance integrated solar combined cycles with minimum modifications to the combined cycle power plant design. Energy Conversion and Management, 111:186–97.

[8] F. I. Abam, M. C. Ndukwu, O. I. Inah, O. D. Uchechukwu, M. Setiyo, O. D. Samuel, R. Uche. Thermodynamic modelling of a novel solar-ORC with bottoming ammonia-water absorption cycle (SORCAS) powered by a vapour compression refrigeration condensate for combined cooling and power, Mechanical Engineering for Society and Industry,.3(2) (2023)93-104.

[9] A. E. Karaca, I. A. Dincer. A new integrated solar energy-based system for residential houses. Energy Conversion and Management, https://doi.org/10.1016/j.enconman.2020.113112.

[10] B Sarkis, V. Zare, Proposal and analysis of two novel integrated configurations for hybrid solar-biomass power generation systems: Thermodynamic and economic evaluation. Energy Conv. Management, 160 (2018). 411-425. https://doi.org/10.1016/j.enconman.2018.01.061,

[11] A. O Abdelhay, H. E. S. Fath, S. Nada. A. Solar-driven Polygeneration system for power, desalination, and cooling. Energy, 198(2020). https://doi.org/10.1016/j.energy.2020.117341.

[12] M. Sharifishourabi, T. Ratlamwala, H. Alimoradiyan, E. Sadeghizadeh. Performance assessment of a multigeneration system based on organic Rankine cycle. Iranian Journal of Science and Technology, Transactions of Mechanical Engineering 3 (2016)225-232.

[13] E. Bellos, C. Tzivanidis, C. Optimization of a solar-driven trigeneration system with nanofluid-based parabolic trough collectors. Energies, 10(2017).848-877.

[14] A. Buonomano, F. Calise, A. Palombo, M. Vicidomini, M. Energy and economic analysis of geothermal–solar trigeneration systems: A case study for a hotel building in Ischia. Applied Energy, 138(2015).224-241.

[15] S. Islam, I. Dincer, B. S. Yilbas, B. S. Energetic and exergetic performance analyses of a solar energy-based integrated system for multigeneration including thermoelectric generators. Energy, 93(2015)1246-1258.

[16] B. Roshanzadeh, A. Asadi, G. Mohan. Technical and economic feasibility analysis of solar inlet air cooling systems for combined cycle power plants. Energies 16(2023)5352–5423. doi:10.3390/en16145352.

[17] K. Owebor, C. O. C. Oko, E. O. Diemuodeke, O. J. Ogorure. Thermoenvironmental and economic analysis of an integrated municipal waste-to-energy solid oxide fuel cell, gas, steam, organic fluid- and absorption refrigeration cycle thermal power plants. Appl. Energy 239(2019)1385–1401. doi: 10.1016/j.apenergy.2019.02.032

[18] U. Sahoo, R. Kumar, P. C. Pant, R. Chaudhary. Development of an innovative Polygeneration process in hybrid solar-biomass system for combined power, cooling and desalination. Appl. Therm. Eng. 120 (2017) 560–567. doi: 10.1016/j.applthermaleng.2017.04.034.

[19] F I. Abam, V. Umeh, E. B. Ekwe, S. O. Effiom, J. Egbe, A. J. AnyandI, J. Enyia4, U. H. Ubauike, M. C. Ndukwu. Thermodynamic and environmental performance of a Kalina-based multigeneration cycle with biomass ancillary firing for power, water and hydrogen production. Future Technology 03 (01) (2024) 40-55.

[20] F. I., Abam, B. B Okon, I. F Edem, M. C Ndukwu, E. B Ekpo, O. E. Diemuodeke, (2023). Environmental assessment and CO2 emissions of Brayton cycle configurations based on exergo-sustainability, economic and ecological efficiency using multi-criteria optimization technique. Future Technology, 3(1) (2023)1–12.

[21] P. Ifaei, A. Ataei, C. Yoo. Thermoeconomic and environmental analyses of a low water consumption combined steam power plant and refrigeration Chillers-Part 2: Thermoeconomic an environmental analysis, Energy Convers Manage, http://dx.doi.org/10.1016/j.enconman.2016.06.030.

[22] A. Bejan, G. Tsatsaronis (1995). Thermal design and optimization. Wiley, New York.

[23] F I. Abam, B. B. Okon, E B Ekwe, J Isaac, S. O Effiom, M. C Ndukwu, O. I. Inah, P. A Ubi, S. Oyedepo, O. S Ohunakin. Thermoeconomic and exergoenvironmental sustainability of a power-cooling organic Rankine cycle with ejector system. e-Prime-Advances in Electrical Engineering, ElectronicsandEnergy2(2022)100064.

[24] M. C. Ndukwu, M. I. Ibeh, P. Etim, C. U. Augustine, I. E. Ekop, A. Leonard, L. Oriaku, F. Abam, B. Lamrani, M. Simo-Tagne, L. Bennamoun. Assessment of eco-thermal sustainability potential of a cluster of low-cost solar dryer designs based on exergetic sustainability indicators and earned carbon credit. Cleaner Energy Systems, 3(2022)100027.

Appendix

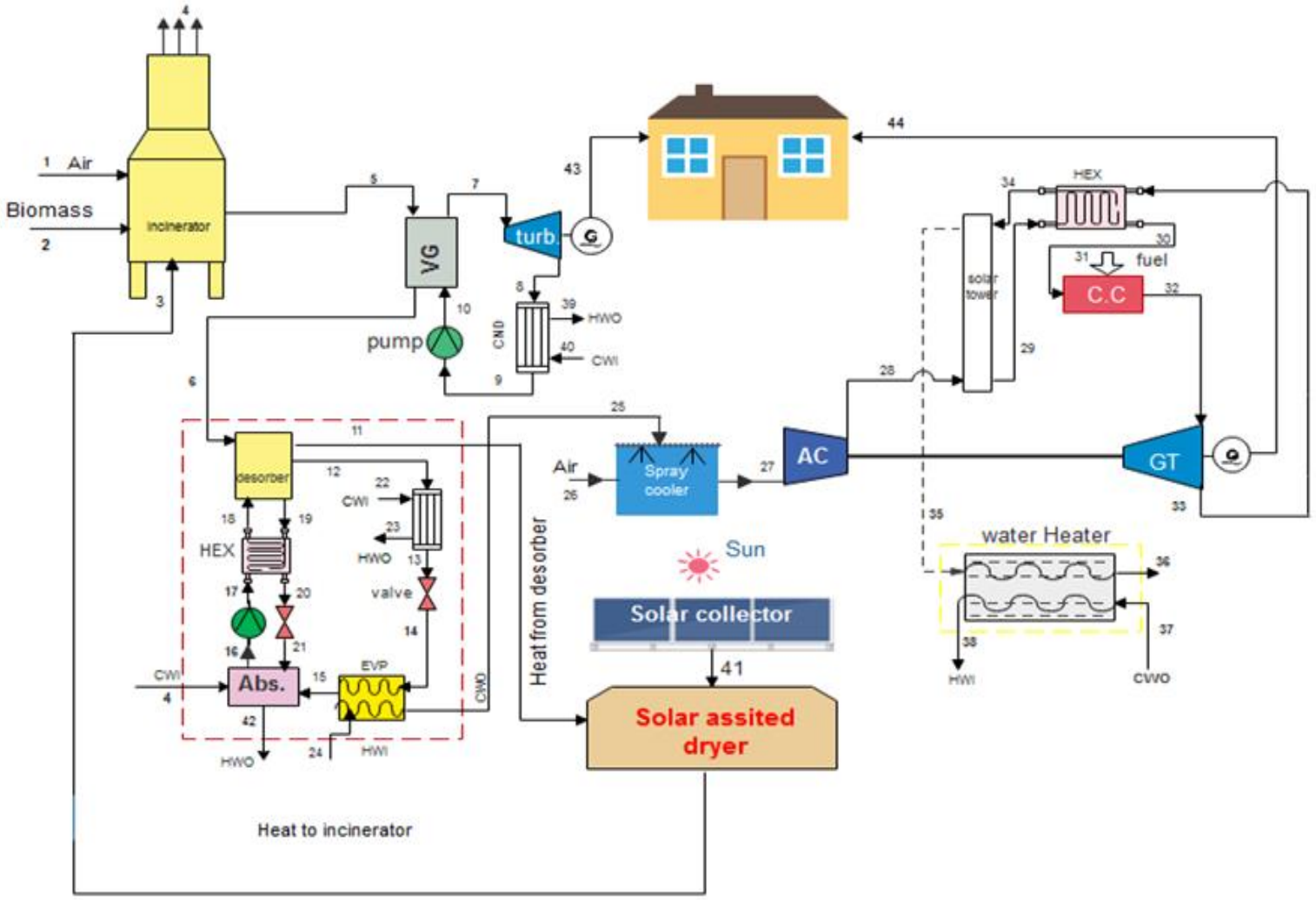

Figure 1. Schematic diagram of the biomass solar-assisted energy systems

Table 1. Energy and exergy balances, as well as exergy of fuel and product for the systems

Component	Energy Balance	Exergy Balance	Exergy of Fuel	Exergy of Product
VAS Desorber	$\dot{m}_6 h_6 + \dot{m}_{18} h_{18} = \dot{m}_{11} h_{11} + \dot{m}_{12} h_{12} + \dot{m}_{19} h_{19}$	$\dot{E}_6 + \dot{E}_{18} = \dot{E}_{11} + \dot{E}_{12} + \dot{E}_{19} + \dot{E}_{D,DES}$	$\dot{E}_6 - \dot{E}_{11} + \dot{E}_{18}$	$\dot{E}_{12} + \dot{E}_{19}$
VAS Hex	$\dot{m}_{17} h_{17} + \dot{m}_{19} h_{19} = \dot{m}_{18} h_{18} + \dot{m}_{20} h_{20}$	$\dot{E}_{17} + \dot{E}_{19} = \dot{E}_{18} + \dot{E}_{20} + \dot{E}_{D,HEX}$	$\dot{E}_{19} - \dot{E}_{20}$	$\dot{E}_{18} - \dot{E}_{17}$
VAS Pump	$\dot{m}_{16} h_{16} + \dot{W}_{Pump} = \dot{m}_{17} h_{17}$	$\dot{E}_{16} + \dot{W}_{Pump} = \dot{E}_{17} + \dot{E}_{D,Pump}$	$\dot{W}_{Pump}$	$\dot{E}_{17} - \dot{E}_{16}$
VAS Absorber	$\dot{m}_{15} h_{15} + \dot{m}_{21} h_{21} + \dot{m}_{in} h_{in} = + \dot{m}_{16} h_{16} + \dot{m}_{out} h_{out}$	$\dot{E}_{15} + \dot{E}_{21} + \dot{E}_{in} = \dot{E}_{16} + \dot{E}_{out} + \dot{E}_{D,ABS}$	$\dot{E}_{21} + \dot{E}_{15}$	$\dot{E}_{16} + \dot{E}_{out} - \dot{E}_{in}$
VAS Valve20/21	$\dot{m}_{20} h_{20} = \dot{m}_{21} h_{21}$	$\dot{E}_{20} = \dot{E}_{21} + \dot{E}_{D,Valve}$	$\dot{E}_{20}$	$\dot{E}_{21}$
VAS Evaporator	$\dot{m}_{14} h_{14} + \dot{m}_{24} h_{24} = \dot{m}_{15} h_{15} + \dot{m}_{25} h_{25}$	$\dot{E}_{14} + \dot{E}_{24} = \dot{E}_{15} + \dot{E}_{25} + \dot{E}_{D,EVP}$	$\dot{E}_{15} - \dot{E}_{14}$	$\dot{E}_{24} - \dot{E}_{25}$
VAS Valve13/14	$\dot{m}_{13} h_{13} = \dot{m}_{14} h_{14}$	$\dot{E}_{13} = \dot{E}_{14} + \dot{E}_{D,Valve}$	$\dot{E}_{13}$	$\dot{E}_{14}$
VAS Condenser	$\dot{m}_{12} h_{12} + \dot{m}_{22} h_{22} = \dot{m}_{13} h_{13} + \dot{m}_{23} h_{23}$	$\dot{E}_{12} + \dot{E}_{22} = \dot{E}_{13} + \dot{E}_{23} + \dot{E}_{D,CND}$	$\dot{E}_{12} - \dot{E}_{13}$	$\dot{E}_{23} - \dot{E}_{22}$
Waste dryer	$\dot{m}_{11} h_{11} + \dot{m}_{41} h_{41} = \dot{m}_{42} h_{42}$	$\dot{E}_{11} + \dot{E}_{41} = \dot{E}_{42} + \dot{E}_{D,Solar\ Dryer}$	$\dot{E}_{11} + \dot{E}_{41}$	$\dot{E}_{42}$
GT Air comp.	$\dot{m}_{27} h_{27} + \dot{W}_{AC} = \dot{m}_{28} h_{28}$	$\dot{E}_{27} + \dot{W}_{AC} = \dot{E}_{28} + \dot{E}_{D,AC}$	$\dot{W}_{AC}$	$\dot{E}_{28} - \dot{E}_{27}$
Solar tower	$\dot{m}_{28} h_{28} + \dot{m}_{34} h_{34} = \dot{m}_{29} h_{29} + \dot{m}_{35} h_{35}$	$\dot{E}_{28} + \dot{E}_{34} = \dot{E}_{29} + \dot{E}_{35} + \dot{E}_{D,Solar\ TW}$	$\dot{E}_{29} - \dot{E}_{28}$	$\dot{E}_{34} - \dot{E}_{35}$
GT Hex	$\dot{m}_{29} h_{29} + \dot{m}_{33} h_{33} = \dot{m}_{30} h_{30} + \dot{m}_{34} h_{34}$	$\dot{E}_{29} + \dot{E}_{33} = \dot{E}_{30} + \dot{E}_{34} + \dot{E}_{D,GT\ HEX}$	$\dot{E}_{33} - \dot{E}_{34}$	$\dot{E}_{30} - \dot{E}_{29}$
GT CC	$\dot{m}_{30} h_{30} + \dot{m}_{31} h_{31} = \dot{m}_{32} h_{32}$	$\dot{E}_{30} + \dot{E}_{31} = \dot{E}_{32} + \dot{E}_{D,GT\ CC}$	$\dot{E}_{30} + \dot{E}_{31}$	$\dot{E}_{32}$
GT Expander	$\dot{m}_{32} h_{32} = \dot{m}_{33} h_{33} + \dot{W}_{GT}$	$\dot{E}_{32} = \dot{E}_{33} + \dot{W}_{GT} + \dot{E}_{D,GT}$	$\dot{E}_{32} - \dot{E}_{33}$	$\dot{W}_{GT}$
Water Heater	$\dot{m}_{35} h_{35} + \dot{m}_{37} h_{37} = \dot{m}_{36} h_{36} + \dot{m}_{38} h_{38}$	$\dot{E}_{35} + \dot{E}_{37} = \dot{E}_{36} + \dot{E}_{38} + \dot{E}_{D,WH}$	$\dot{E}_{38} - \dot{E}_{37}$	$\dot{E}_{35} - \dot{E}_{36}$

Table 2. Component cost and auxiliary equations

Component	Exergoeconomic balance	Auxiliary equation
Incinerator	$\dot{C}_1 + \dot{C}_2 + \dot{C}_3 + \dot{Z}_{Incin.} = \dot{C}_5$	Nil
Vapour Gen.	$\dot{C}_5 + \dot{C}_{10} + \dot{Z}_{VG} = \dot{C}_6 + \dot{C}_7$	$\dot{C}_5\dot{E}_6 - \dot{C}_6E_5 = 0$
ORC Turb	$\dot{C}_7 + \dot{Z}_{TURB} = \dot{C}_8 + \dot{C}_{\dot{W}_{TURB}} + \dot{C}_{\dot{W}VAS_{Pump}} + \dot{C}_{\dot{W}_{ORC\,Pump}}$	$\dot{C}_7\dot{E}_8 - \dot{C}_8E_7 = 0$ $\dot{C}_{\dot{W}_{TURB}}\dot{W}_{ORC\,Pump} - \dot{C}_{\dot{W}_{ORC\,Pump}}\dot{W}_{TURB} = 0$ $\dot{C}_{\dot{W}_{TURB}}\dot{W}VAS_{Pump} - \dot{C}_{\dot{W}VAS_{Pump}}\dot{W}_{TURB} = 0$
ORC Cond.	$\dot{C}_8 + \dot{C}_{40} + \dot{Z}_{CND} = \dot{C}_9 + \dot{C}_{39}$	$\dot{C}_8\dot{E}_9 - \dot{C}_9E_8 = 0$
ORC Pump	$\dot{C}_9 + \dot{C}_{\dot{W}_{ORC\,Pump}} + \dot{Z}_{Pump} = \dot{C}_{10}$	-
VAS Desorber	$\dot{C}_6 + \dot{C}_{18} + \dot{Z}_{DES} = \dot{C}_{11} + \dot{C}_{12} + \dot{C}_{19}$	$\dot{C}_6\dot{E}_{11} - \dot{C}_{11}E_{12} = 0$ $\dot{C}_{19}\dot{E}_{12} - \dot{C}_{12}E_{19} = 0$
VAS Hex	$\dot{C}_{17} + \dot{C}_{19} + \dot{Z}_{HEX} = \dot{C}_{18} + \dot{C}_{20}$	$\dot{C}_{19}\dot{E}_{20} - \dot{C}_{20}E_{19} = 0$
VAS Pump	$\dot{C}_{16} + \dot{C}_{\dot{W}_{VAS\,Pump}} + \dot{Z}_{Pump} = \dot{C}_{17}$	-
VAS Absorber	$\dot{C}_{15} + \dot{C}_{21} + \dot{C}_{in} + \dot{Z}_{ABS} = \dot{C}_{16} + \dot{C}_{out}$	$\dot{C}_{out}\dot{E}_{in} - \dot{C}_{in}E_{out} = 0$
VAS Valve20/21	$\dot{C}_{20} + \dot{Z}_{Valve} = \dot{C}_{21}$	-
VAS Evaporator	$\dot{C}_{14} + \dot{C}_{24} + \dot{Z}_{EVP} = \dot{C}_{15} + \dot{C}_{25}$	$\dot{C}_{24}\dot{E}_{25} - \dot{C}_{25}E_{24} = 0$
VAS Valve13/14	$\dot{C}_{13} + \dot{Z}_{Valve} = \dot{C}_{14}$	Nil
VAS Condenser	$\dot{C}_{12} + \dot{C}_{22} + \dot{Z}_{CND} = \dot{C}_{13} + \dot{C}_{23}$	$\dot{C}_{12}\dot{E}_{13} - \dot{C}_{13}E_{12} = 0$
Waste dryer	$\dot{C}_{11} + \dot{C}_{41} + \dot{Z}_{Solar\,Dryer} = \dot{C}_{42}$	-
GT Air comp.	$\dot{C}_{27} + \dot{C}_{\dot{W}_{AC}} + \dot{Z}_{AC} = \dot{C}_{28}$	-
Solar tower	$\dot{C}_{28} + \dot{C}_{34} + \dot{Z}_{Solar\,TW} = \dot{C}_{29} + \dot{C}_{35}$	$\dot{C}_{34}\dot{E}_{35} - \dot{C}_{35}E_{34} = 0$
GT Hex	$\dot{C}_{29} + \dot{C}_{33} + \dot{Z}_{GT\,HEX} = \dot{C}_{30} + \dot{C}_{34}$	$\dot{C}_{33}\dot{E}_{34} - \dot{C}_{34}E_{33} = 0$
GT CC	$\dot{C}_{30} + \dot{C}_{31} + \dot{Z}_{GT\,CC} = \dot{C}_{32}$	Nil
GT Expander	$\dot{C}_{32} + \dot{Z}_{GT} = \dot{C}_{33} + \dot{C}_{\dot{W}_{GT}} + \dot{C}_{\dot{W}_{AC}}$	$\dot{C}_{32}\dot{E}_{33} - \dot{C}_{33}E_{32} = 0$ $\dot{C}_{\dot{W}_{GT}}\dot{W}_{AC} - \dot{C}_{\dot{W}_{AC}}\dot{W}_{GT} = 0$
Water Heater	$\dot{C}_{35} + \dot{C}_{37} + \dot{Z}_{WH} = \dot{C}_{36} + \dot{C}_{38}$	$\dot{C}_{35}\dot{E}_{36} - \dot{C}_{36}E_{35} = 0$

Table 3. Component cost functions, cost of product, and cost of fuel

Component	Cost function (PEC)	Cost of product	cost of fuel
Incinerator	$2.9 \times 10^6 \lvert 3.6\dot{m}_2 \rvert^{0.7}$	$\dot{C}_5$	$\dot{C}_1 + \dot{C}_2 + \dot{C}_3 + \dot{C}_{42}$
Vapour Gen.	$130 \left\lvert \frac{A_{VAS_{HEX}}}{0.093} \right\rvert^{0.78}$	$\dot{C}_7 - \dot{C}_{10}$	$\dot{C}_5 - \dot{C}_6$
ORC Turb	$4750 \lvert \dot{W}_{ORC_{Turb}} \rvert^{0.75}$	$\dot{C}_{WORC,TUB} + \dot{C}_{WORC,PUM} + \dot{C}_{WVAS,PUM}$	$\dot{C}_7 - \dot{C}_8$
ORC Cond.	$516.62 \left\lvert \frac{\dot{Q}_{ORC\ CND}}{0.15\Delta T_{ORC\ CND}} \right\rvert$	$\dot{C}_{39} - \dot{C}_{40}$	$\dot{C}_8 - \dot{C}_9$
ORC Pump	$705.5 \left\lvert 0.00\dot{1}W_{ORC_{Pump}} \right\rvert^{0.71} \left\lvert 1 + \frac{0.2}{1-\eta_P} \right\rvert$	$\dot{C}_{10} - \dot{C}_9$	$\dot{C}_{WORC,PUM}$
VAS Desorber	$130 \left\lvert \frac{A_{VAS_{DES}}}{0.093} \right\rvert^{0.78}$	$\dot{C}_{19} + \dot{C}_{12}$	$\dot{C}_6 - \dot{C}_{11} + \dot{C}_{18}$
VAS Hex	$130 \left\lvert \frac{A_{VAS_{HEX}}}{0.093} \right\rvert^{0.78}$	$\dot{C}_{18} - \dot{C}_{17}$	$\dot{C}_{19} - \dot{C}_{20}$
VAS Pump	$100 \left\lvert \frac{\dot{W}_{VAS_{Pump}}}{100} \right\rvert^{0.26} \left\lvert \frac{1-\eta_P}{\eta_P} \right\rvert^{0.5}$	$\dot{C}_{17} - \dot{C}_{16}$	$\dot{C}_{WVAS,PUM}$
VAS Absorber	$130 \left\lvert \frac{A_{VAS_{ABS}}}{0.093} \right\rvert^{0.78}$	$\dot{C}_{16} + \dot{C}_{W,out}$	$\dot{C}_{15} - \dot{C}_{21} + \dot{C}_{W,in}$
VAS Valve20/21	$37 \left\lvert \frac{P_{20}}{P_{21}} \right\rvert^{0.68}$	$\dot{C}_{21}$	$\dot{C}_{20}$
VAS Evaporator	$130 \left\lvert \frac{A_{VAS_{EVP}}}{0.093} \right\rvert^{0.78}$	$\dot{C}_{15} - \dot{C}_{14}$	$\dot{C}_{24} - \dot{C}_{25}$
VAS Valve13/14	$37 \left\lvert \frac{P_{13}}{P_{14}} \right\rvert^{0.68}$	$\dot{C}_{14}$	$\dot{C}_{13}$
VAS Condenser	$1773\dot{m}_{12}$	$\dot{C}_{23} - \dot{C}_{22}$	$\dot{C}_{12} - \dot{C}_{13}$
Waste dryer	$130 \left\lvert \frac{A_{VAS_{EVP}}}{0.093} \right\rvert^{0.78}$	$\dot{C}_{QDrayer}$	$\dot{C}_{11} - \dot{C}_{42} + \dot{C}_{41}$
GT Air comp.	$\frac{39.5\dot{m}_f}{0.9-\eta_{AC}} \left\lvert \frac{P_{28}}{P_{27}} \right\rvert ln \left\lvert \frac{P_{28}}{P_{27}} \right\rvert$	$\dot{C}_{28} - \dot{C}_{27}$	$\dot{C}_{GT,AC}$
Solar tower	$130 \left\lvert \frac{A_{ST}}{0.093} \right\rvert^{0.78}$	$\dot{C}_{29} - \dot{C}_{28}$	$\dot{C}_{34} - \dot{C}_{35}$
GT Hex	$130 \left\lvert \frac{A_{GT_{HEX}}}{0.093} \right\rvert^{0.78}$	$\dot{C}_{30} - \dot{C}_{29}$	$\dot{C}_{34} - \dot{C}_{33}$
GT CC	$\left(\frac{46.08\dot{m}_{30}}{0.995 - \frac{P_{32}}{P_{30}}} \right) \lvert 1 + exp(0.018T_{32} - 26.4) \rvert$	$\dot{C}_{32}$	$\dot{C}_{30} + \dot{C}_{31}$
GT Expander	$\left\lvert \frac{479.34\dot{m}_{32}}{0.92-\eta_T} \right\rvert ln \left\lvert \frac{P_{32}}{P_{33}} \right\rvert \lvert 1 + exp[0.036T_{32} - 54.4] \rvert$	$\dot{C}_{WTnet} + \dot{C}_{W,GT\ AC}$	$\dot{C}_{32} - \dot{C}_{33}$